Electronic Supplementary Information

Additive-controlled synthesis of monodisperse single crystalline gold nanoparticles: interplay of shape and surface plasmon resonance

Felizitas Kirner[a], Pavel Potapov[b], Johannes Schultz[b], Jessica Geppert[a], Magdalena Müller[a], Guillermo González-Rubio[a], Sebastian Sturm[b], Axel Lubk[b], Elena Sturm[a]*

[a] Department of Chemistry, University of Konstanz, Universitätsstr. 10, D-78457 Konstanz, Germany

**E-Mail: elena.sturm@uni-konstanz.de*

[b] Institute for Solid State Research, Leibniz Institute for Solid State and Materials Research Dresden, Helmholtzstraße 20, 01069 Dresden, Germany

Reaction parameters

Table S1. Reaction parameters for the growth of gold NPs with adjustable ratio of the cubic {100} and the octahedral {111} facets. If not mentioned otherwise, the reaction was performed as described in the methods section.

Figure	*KBr 0.1 M [µL]*	*AA 0.1 M [µL]*	*Spherical seeds [µL]*	*water [mL]*	*CPC [mM]*	*KBr [mM]*	*AA [mM]*
2a	200	750	3000		84.9	0.7	2.5
2b	400	750	1000		90.4	1.4	2.7
2c	1000	750	500		90.1	3.6	2.7
2d	2400	750	200		86.7	8.3	2.6
3a	625*	750	200		86.4	8.6	2.6
3b	1125*	750	200		80.8	14.5	2.4
3c	1625*	750	200		75.9	19.7	2.3
3d	2125*	750	200		71.5	24.3	2.1
4.1	125*	1750	1000	0.63	86.2	1.7	6.0
4.2	625*	1750	1000	0.13	86.2	8.6	6.0
4.3	1250*	1750	1000	0.00	86.2	17.2	6.0
4.4	125*	750	1000	1.63	86.2	1.7	2.6
4.5	625*	750	1000	1.13	86.2	8.6	2.6
4.6	1250*	750	1000	0.50	86.2	17.2	2.6
4.7	125*	250	1000	2.13	86.2	1.7	0.9
4.8	625*	250	1000	1.63	86.2	8.6	0.9
4.9	1250*	250	1000	1.00	86.2	17.2	0.9
4.10	0*	750	1000	1.75	86.2	0.0	2.6
S3a	500	750	1000		90.1	1.8	2.7
S3b	500	750	500		91.7	1.8	2.8
S3c	500	750	200		92.8	1.9	2.8
S4a	2500	750	1000		84.0	8.4	2.5
S4b	2500	750	750		84.7	8.5	2.5
S4c	2500	750	500		85.5	8.5	2.6
S4d	2500	750	400		85.8	8.6	2.6
S4e	2500	750	300		86.1	8.6	2.6
S4f	2500	750	200		86.4	8.6	2.6
S4g	2500	750	100		86.7	8.7	2.6
S4h	2500	750	50		86.8	8.7	2.6
S6a	500	750	1000		90.1	1.8	2.7
S6b	500	750	400		92.1	1.8	2.8
S6c	2500	750	1000		84.0	8.4	2.5
S6d	2500	750	400		85.8	8.6	2.6
S7a	0	750	200		94.5	0.0	2.8
S7b	625*	750	200		86.4	8.6	2.6
S7c	1125*	750	200		80.8	14.5	2.4
S7d	1625*	750	200		75.9	19.7	2.3
S7e	2125*	750	200		71.5	24.3	2.1
S7f	1125*	1750	200		78.2	14.1	5.5
S7g	1125*	250	200		82.1	14.8	0.8
S8a	0	750	1000		91.7	0.0	2.8
S8b	2000	750	1000		85.5	6.8	2.6
S8c	4000	750	1000		80.0	12.8	2.4
S8d	6000	750	1000		75.2	18.0	2.3
S8e	2000	1750	1000		82.6	6.6	5.8
S8f	2000	250	1000		87.0	7.0	0.9

*0.4 M KBr

Synthesis and characterization of seed particles

Initial seeds. The synthesis conditions for the initial seed are optimized for a short nucleation time and little crystal growth meaning a rapid reduction of Au^{3+} with $NaBH_4$. This ensures a high yield of single crystalline particles. The synthesis of the initial seed particles follows previously reported procedures.[1-6] The statistics of these seeds are not further relevant to the current publication and will therefore not be discussed more thoroughly. Discussions about the quality and nature of these seeds may be found in other literature.

Spherical seeds. The three samples are prepared from 100 µl, 200 µl and 500 µl initial seeds. TEM images were used to determine the mean diameter of the synthesized spheres. Statistics are done using Fiji.[7] The mean diameter of the samples are 14.9 nm, 12.7 nm, and 9.5 nm, respectively. AUC proved a narrow PDI of 1.04 or less (**Figure S1**). The single crystallinity was proven by overgrowth of Ag on the spheres and following TEM imaging and statistics. Single crystalline spheres will yield cubic Au@Ag particles[1, 8] Spheres can be produced with over 85 % single crystallinity percentage (**Figure S2**) independently from their size. We show that the volume of the spherical seeds scales directly with the amount of initial seeds. Accordingly, the number concentration of spheres can be tuned by adjusting their size. As a surfactant exchange is required for the further synthesis, this can be used to adapt the procedure to available centrifugational techniques (larger spheres sediment at less RPM). In a further growth step, double amount of spheres dispersion with half the volume is needed (**Figure S3**). All investigated sizes of spherical seeds are suited for the synthesis of anisotropic particles if their number is adjusted.

Procedure for the measurement of the kinetics.

The kinetic measurements were carried out as followed. The UV-Vis spectrometer was tempered to 27 °C. A baseline was measured against water. A mixture of 86.2 mM CPC, 17.2 mM KBr, 17.2 µM $HAuCl_4$ and 0.9 mM AA in water was prepared to show a complete reduction of Au^{3+} species to Au^{+} so that this process may be disregarded for the evaluation. These conditions were chosen exemplarily as the most extreme ones used for the kinetics. A reference measurement A_0 of spherical seeds diluted to their final concentration in a CPC/KBr/water solution was measured to have a reliable absorbance spectrum to the beginning of the growth at t_0 for the whole wavelength interval. For the kinetic measurement, the scan rate was adjusted to 800 nm/min (13.33 nm/s) measuring from 800-400 nm in 30 s intervals. Spectra were recorded for a timeframe of 29.5 min.

The growth solution was prepared as described in the Experimental Section. CPC and KBr solution were tempered to 27 °C, $HAuCl_4$ and AA were added. The measurement was started upon addition of the spherical seeds to the growth solution, then 3 mL of this mixture was filled into the spectrometer. Therefore, the wavelength from roughly 800-600 nm of the first measurement were discarded due to artifacts (filling, bubbles).

The maxima of the measured spectra were identified, and the exact measurement time of the maximum was calculated as following: Measurement started at starting time t_0 (0 s, 30 s, ...). The wavelength was measured from 800 nm decreasing with a rate of 800 nm/min (13,33 nm/s). t_{max}, the time when the maximum absorption A_{max} was calculated as t_{max} [s]=t_0 [s]+(800 [nm] - A_{max} [nm])/(13,33 [nm/s]). As the maximum shifts, slightly deviating measurement intervals occurred but were considered in the evaluation. TEM samples were prepared from the growth solution after 30 min.

The growth kinetic of particles of different size and morphologies is investigated using UV-Vis spectroscopy. The kinetic data were evaluated using the adjusted Finke-Watzky (FW) autocatalytic two-step mechanism which allowed to estimate the k_1 and k_2 rate constants of the "pseudoelementary" reactions of reduction of gold ions and growth process NPs with deferent shape. For each investigated system, the rate curves were platted as a function of A_t (at λ_{max} of SPR band; has max. between ~ 520 nm and 570 nm, depending on NPs system, Figure S9) vs. time (t).The rates constants k_1 and k_2 were calculated by fitting the rates curves using the procedure described by Tatarchuk et al.[9-11] In this case, the following equations were used:

$$\frac{d(A_{max} - A_t)}{dt} = a_1(A_{max} - A_t) + a_2(A_{max} - A_t)^2$$

$$\ln(A_{max} - A_t) = a_0 + a_1 x + a_2 x$$

Where $a_0 = \ln(A_{max} - A_0)$, $x_1 = t$, $x_2 = \int (A_{max} - A_t)dt$

This linear regression was used to fit the experimental kinetic curves (using first ln-linearization and afterwards back exp-conversion) and calculate the rates constants k_1 [s^{-1}] and k_2 [$M^{-1}s^{-1}$].

$$k_1 = -\{a_1 + a_2 exp(a_0)\}$$

$$k_2 = l\varepsilon_0 a_2$$

Where $l = 1\ cm$, $\varepsilon_0 = 4.41 \times 10^3\ M^{-1}\ cm^{-1}$ *(for Au NPs)*

The calculated parameters of the linear regression and observed rate constants are listed in Tables in **Figures S6 and S15**.

Assembly of superstructures

5 mL of as prepared nanoparticle dispersion were centrifuged at 9 000 RPM for 5 min. The supernatant was discarded, and the particles were redispersed in 15 mL 0.02 M CPC solution. The dispersion was again centrifuged at 9 000 RPM for 5 min and concentrated to 100 µL. 10 µL of this concentrated dispersion were dropped on a Silicon wafer (orientation <100>, Siegert Wafer) and dried under ambient conditions. The dried samples were then treated by plasma cleaning for 15 min to enhance the quality of electron imaging.

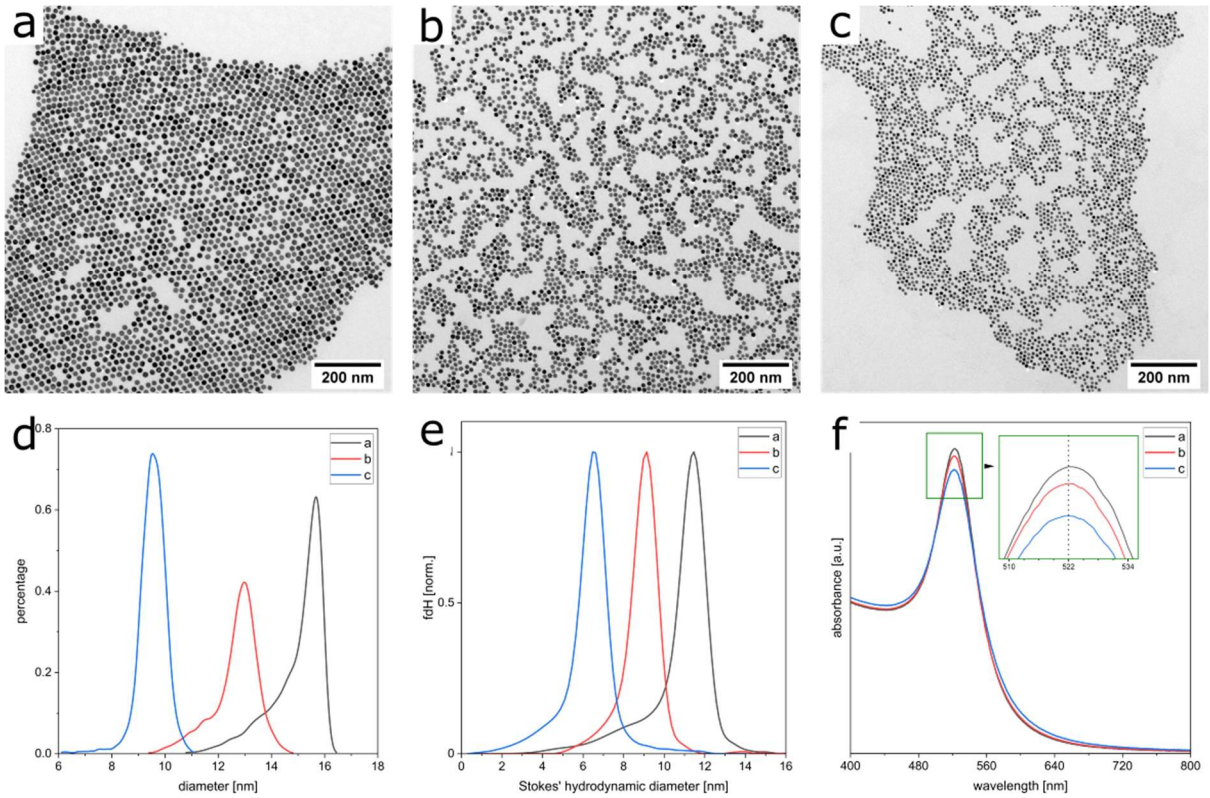

Figure S1. Characterization of gold nanospheres. TEM images spherical seeds from (a) 100 µl, (b) 200 µl and (c) 500 µl initial seeds. (d) UV-Vis spectroscopy shows that no agglomerates are present. The maximum absorbance of the spheres is 522 nm for all synthesized sizes. (e) TEM images were used to determine the mean diameter of the synthesized spheres. Statistics were done using Fiji.[7] The mean diameter of the samples are 14.9 nm, 12.7 nm, and 9.5 nm, respectively. (e) To circumvent bias by sample preparation for TEM, AUC is used to determine the polydispersity of the crude samples. The PDI was calculated as the ratio of the weight average and number average. The PDI is 1.02, 1.01, and 1.04 for Samples 1, 2 and 3, respectively. (f) UV-Vis spectroscopy shows an absorbance maximum for all three samples at 522 nm.

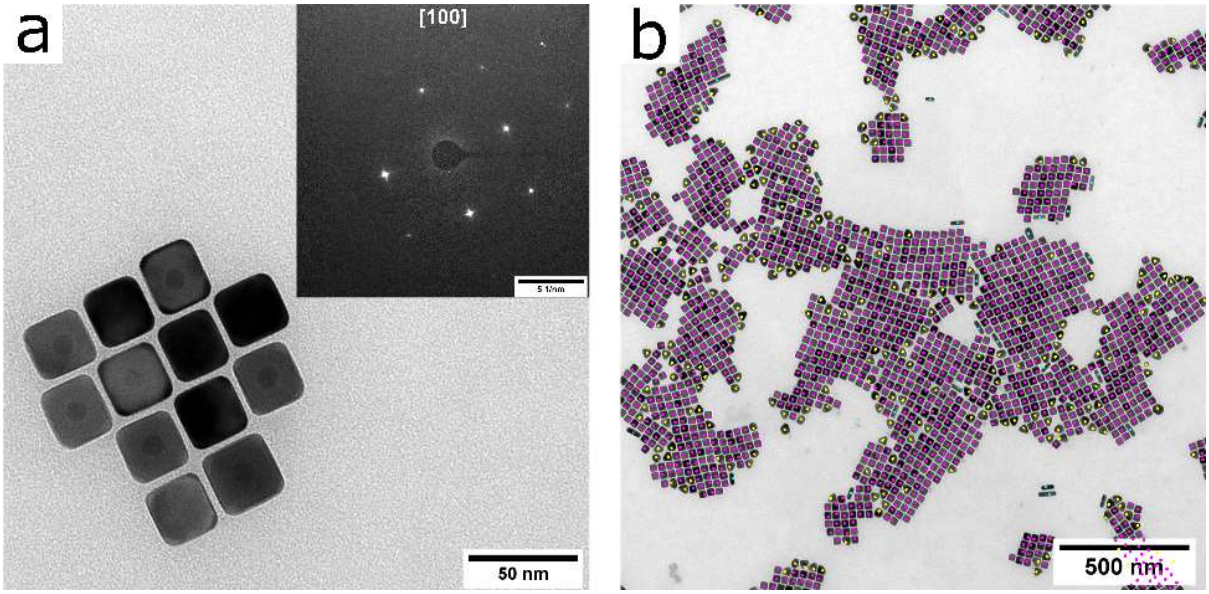

Figure S2. Characterization of gold nanospheres. The share of single crystalline spheres exceeds 85 %. The single crystalline nature of the spheres is investigated using the overgrowth of Ag on the spheres. Single crystalline spheres will yield cubic Au@Ag particles. (a) Exemplary TEM image of silver particles grown from previously synthesized spheres from Figure S1c. The according ED pattern prove the single crystalline nature of these cubes. (b) Pink dots indicate cubic Au@Ag particles and therefore single crystalline spheres. Yellow stars indicate spherical or prismatic structures and thereby twinned Au spheres. Blue squares indicate rod like Au@Ag particles and a penta-twinning in the Au spheres.

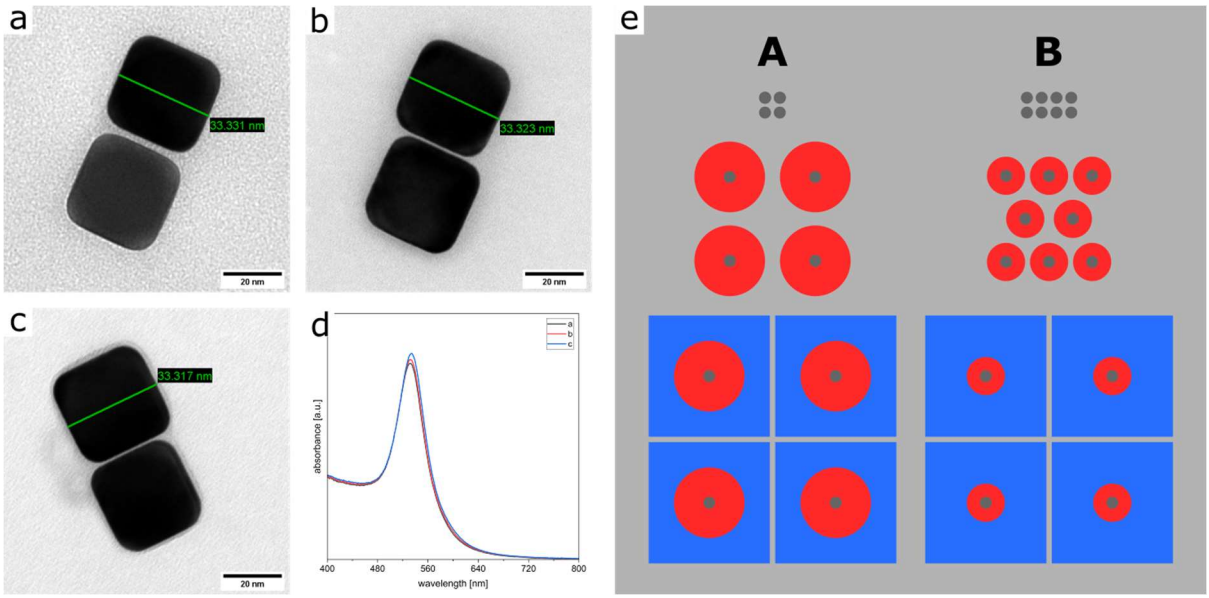

Figure S3. Characterization of gold nanospheres. The size of the nanospheres that are used as spherical seeds has no influence on the outcome of the faceting of the anisotropic particles. The only influence seems to be their number concentrations. Three NP synthesis were conducted under same conditions with only a change in volume of the spherical spheres depicted in Figure S1a-c. Washing was not carried out as not to change the particle concentration. TEM images from NP synthesized from (a) 1000 µL S1a, (b) 500 µL S1b, and (c) 200 µL S1c yield NP with nearly the same edge length of 33 nm. (d) The UV-Vis spectrum confirms the monodispersity in size and shape. Synthesis conditions are supplied in Table 1. (e) More thorough explanation of the above, from top to bottom: Different volumes of initial seeds (4 in A and 8 in B) are added to the same amount of Au^{3+}. This results in spherical seeds with a particle concentration that scales with the amount of added initial seeds. $2 \cdot c(A) = c(B)$ respectively ($2 \cdot 4 = 8$). The particle volume is adjusted accordingly. For the further grow, the number of spherical seeds can be adjusted with the volume of dispersion. V(A) and 0.5 V(B) contain the same number of spherical seeds (here 4). The resulting faceted particles have the same size.

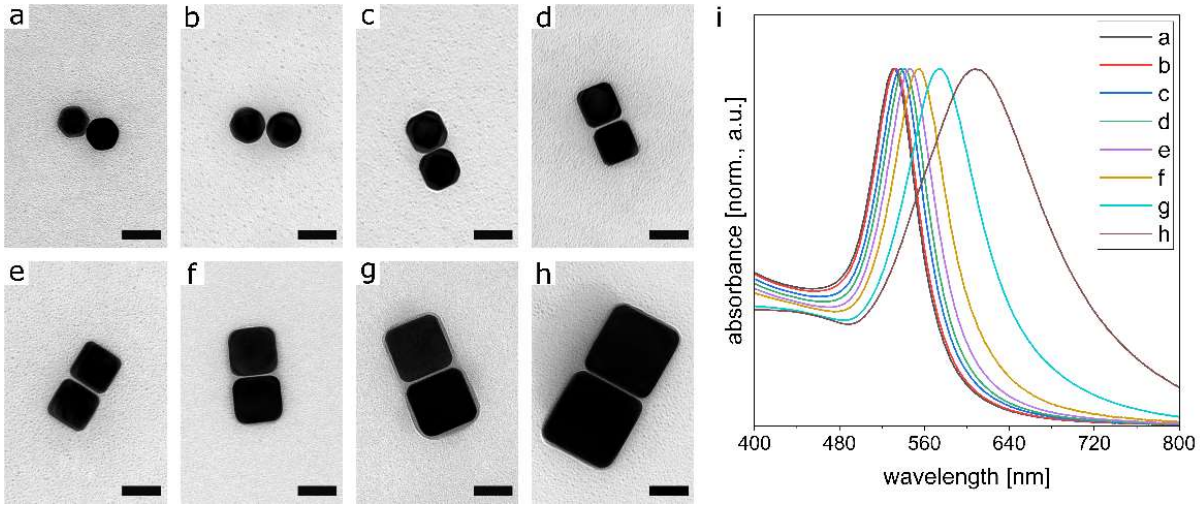

Figure S4. By changing the number of spherical seeds in the NP growth while leaving the remaining conditions as is, the growth process and the protection of the different facets can be estimated. (a-h) TEM images of NPs synthesized with decreasing amount of seed particles. The minimum diameter changes from 40 nm to 100 nm. Scale bar is 50 nm. (i) Normalized UV-Vis absorbance spectra for the respective particles in (a-h) show the expected red shift for particles of increasing size. Synthesis conditions are found in Table S1.

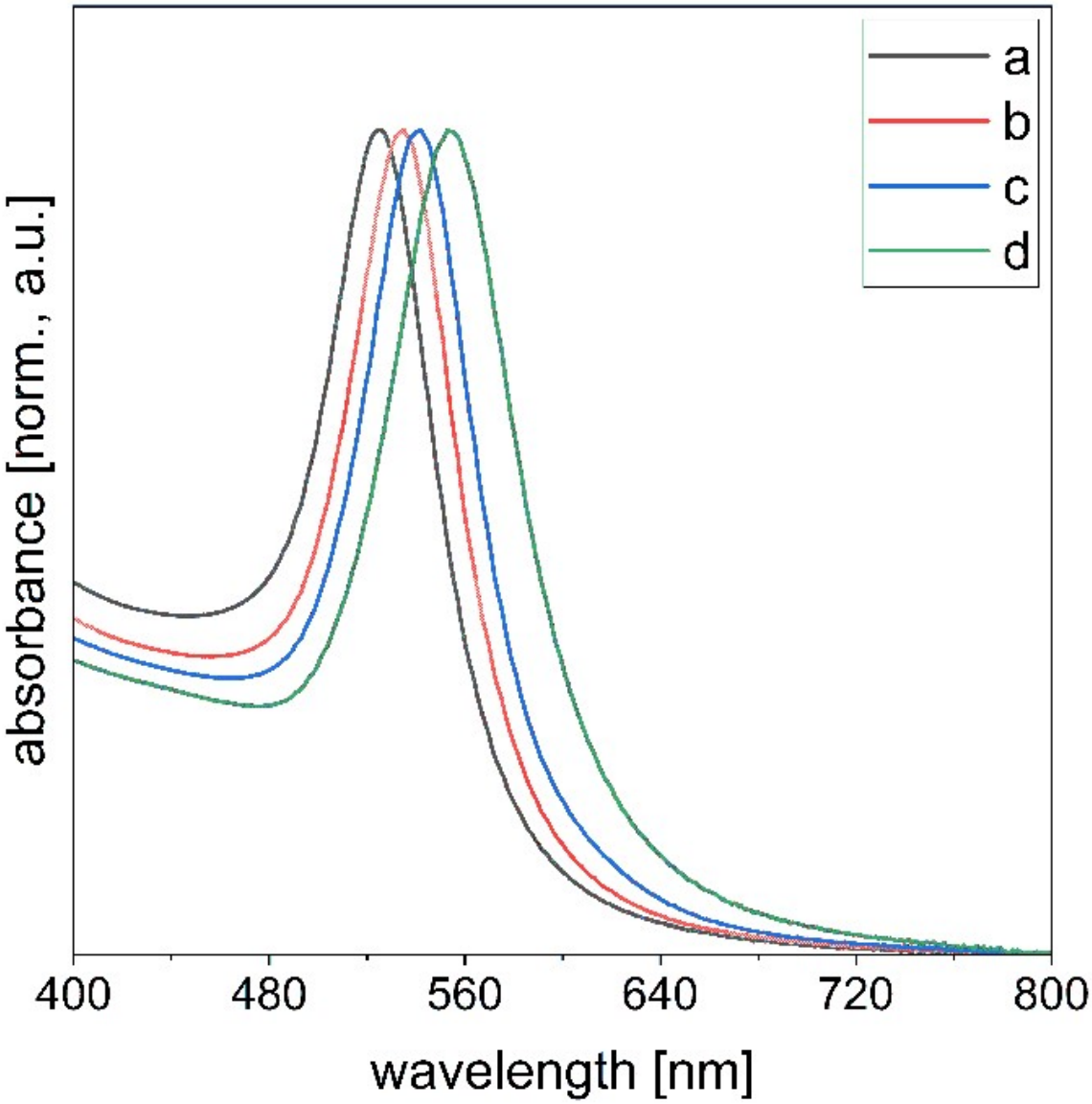

Figure S5. UV-Vis spectra of the cubes of different edge lengths (Figure 2) show a red shift for increasing edge lengths. The monodispersity in size and shape reflects in a narrow bandwidth.

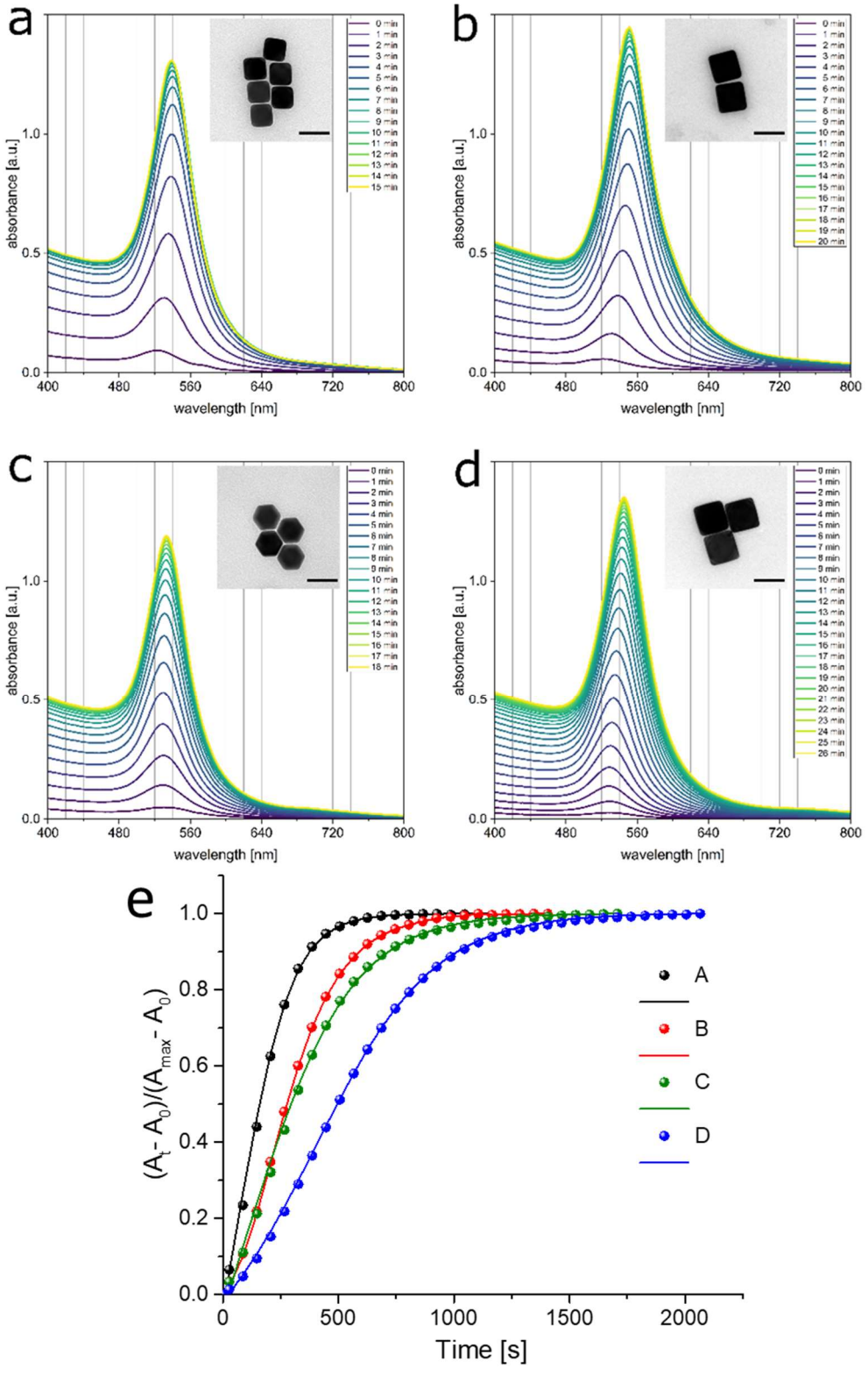

Sample No	a_0	a_1	a_2	$s(a_0)$	$s(a_0)$	$s(a_0)$	R^2	k_1	k_2
A	0.29831	-0.00898	0.00434	0.04700	0.00012	0.00039	0.99899	0.00313	19.14
B	0.37748	-0.00643	0.00346	0.33120	0.00008	0.00017	0.99908	0.00138	15.26
C	0.2375	-0.00446	0.00208	0.02500	0.00009	0.00019	0.99865	0.00182	9.17
D	0.32885	-0.00391	0.00231	0.00652	0.00003	0.00004	0.99980	0.00070	10.19

Figure S6. The kinetics of particle growth can be observed using UV-Vis spectroscopy. Different numbers of spherical seeds are added to a synthesis with otherwise same growth conditions. It can be observed that larger particles take slightly longer to finish their growth process. In addition to minutely spectra, a TEM image of the final NPs is supplied. Synthesis conditions are found in Table S1. Growth in a solution with 1.8 mM KBr with (a) 1000 µL and (b) 400 µL sphere dispersion. Synthesis results in nanocubes with edge lengths of 37 nm and 48 nm, respectively. (c) If KBr concentrations are chosen five times higher, smaller particles from 1000 µL sphere dispersion grow distinctly more truncated. (d) Growth under the same conditions but with 400 µL sphere dispersion grow again to more cubic structures. (d) Normalized rate curves at λ_{max} obtained from UV-Vis spectra shown in A-D. Points – experimental data; straight lines – fitted curves by Finke-Watzky autocatalytic two-step model based on procedure describes by Tatarchuk et al.[9-11] The calculated parameters of fitted curves (a_0, a_1, a_2, their standard deviations (s), and R^2) and k_1 and k_2 rate constants of the "pseudoelementary" reactions are listed in the table.

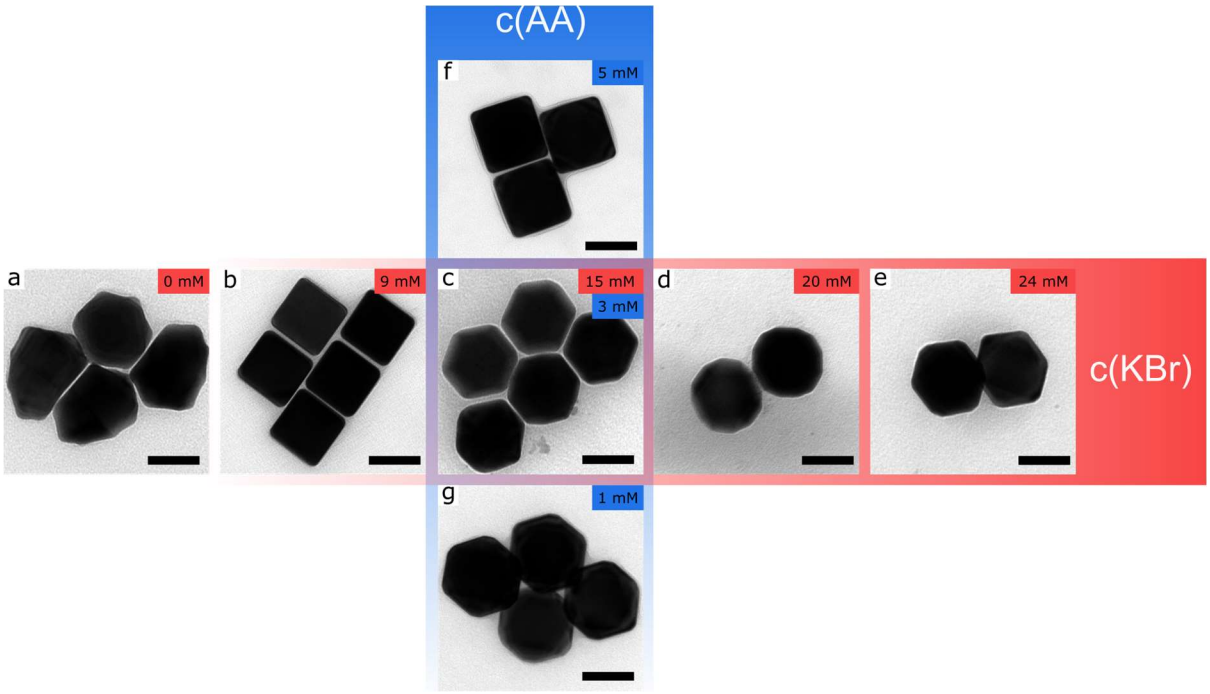

Figure S7. The crystal habit of cubic {100} and octahedral {111} facets can be changed by adjusting the concentrations of KBr and AA. Exemplary TEM images of particles synthesized from 200 µL spheres are provided. This corresponds to an edge length of 60 nm for the most cubic particles (b). (a) No defined faceting is developed without presence of KBr in the synthesis mixture. (b-e) The {100} facets develop more pronounced in the presence of low KBr concentrations while the {111} facets become more dominant with increasing concentrations. (f, c, g) The concentration of AA seems to have the opposite influence. Higher concentrations lead to more pronounced {100} facets. Scale bar is 50 nm for all images. Synthesis conditions are found in Table S1.

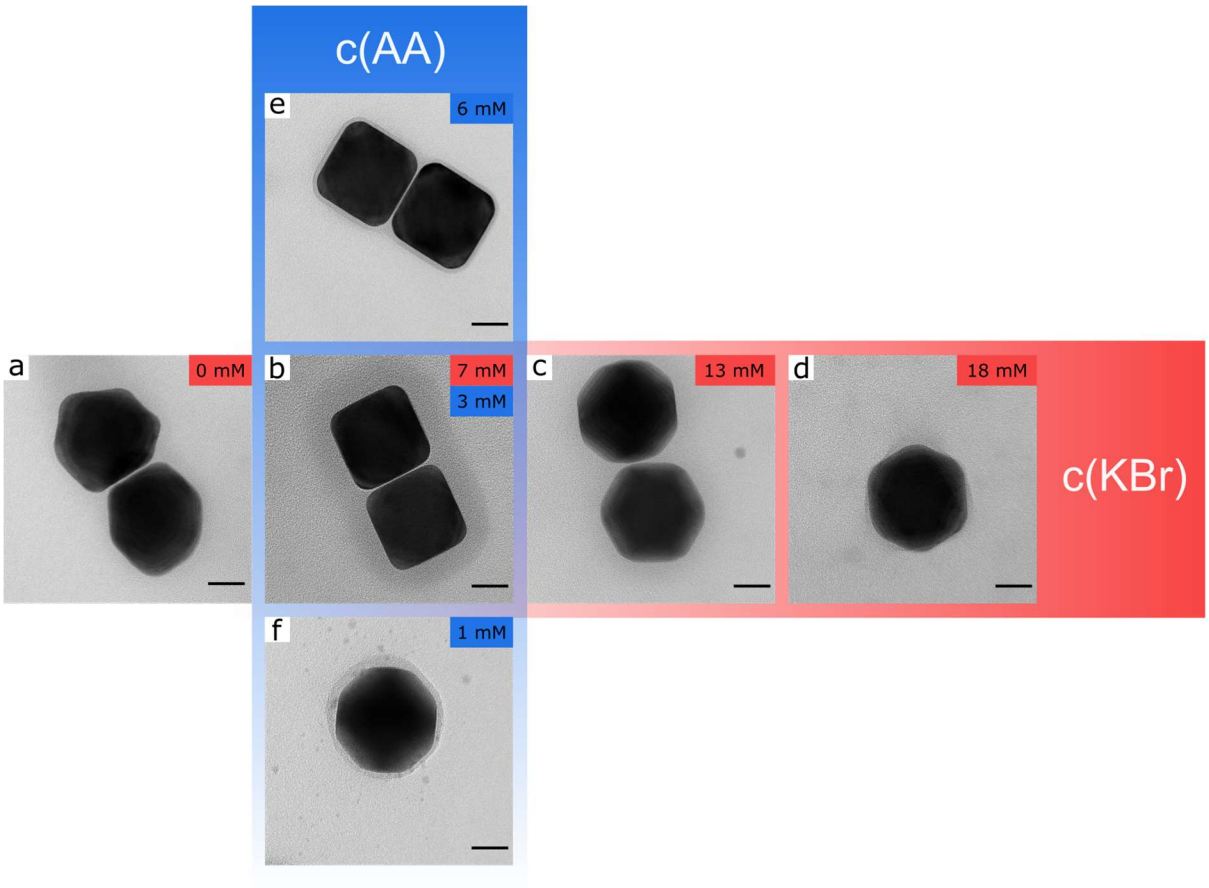

Figure S8. The crystal habit of cubic {100} and octahedral {111} facets can be changed by adjusting the concentrations of KBr and AA. Exemplary TEM images of particles synthesized from 1000 µL spheres are provided. This corresponds to an edge length of 45 nm for the most cubic particles (b). (a) No defined faceting is developed without presence of KBr in the synthesis mixture. (b-d) The {100} facets develop more pronounced in the presence of low KBr concentrations while the {111} facets become more dominant with increasing concentrations. (e, b, f) The concentration of AA seems to have the opposite influence. Higher concentrations lead to more pronounced {100} facets. Scale bar is 25 nm for all images. Synthesis conditions are found in Table S1.

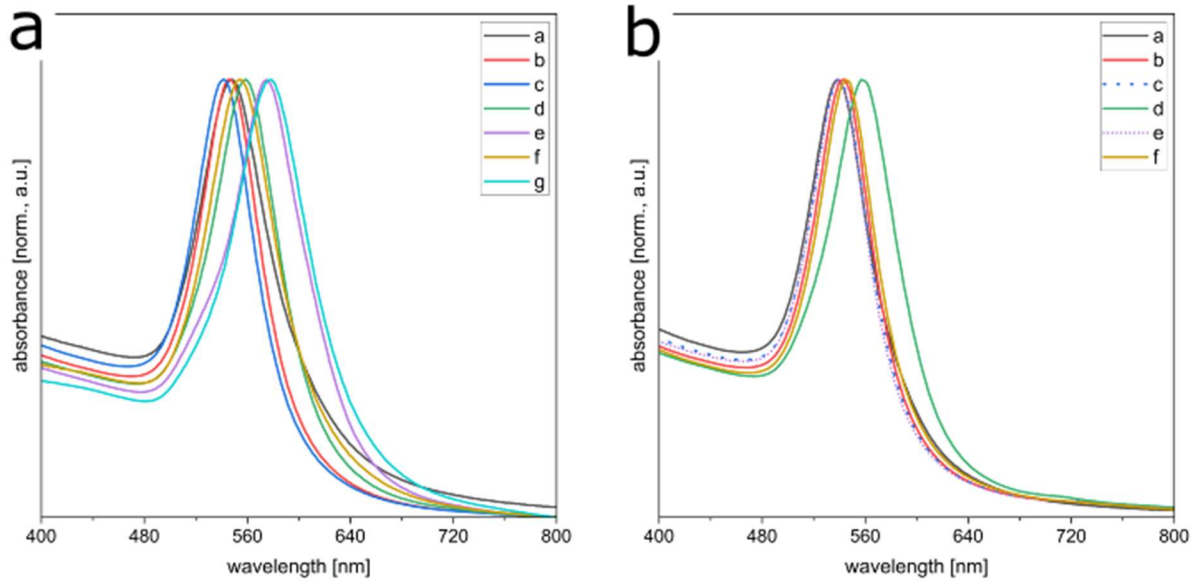

Figure S9. UV-Vis spectra for the particles depicted in Figure (a) S7 and (b) S8.

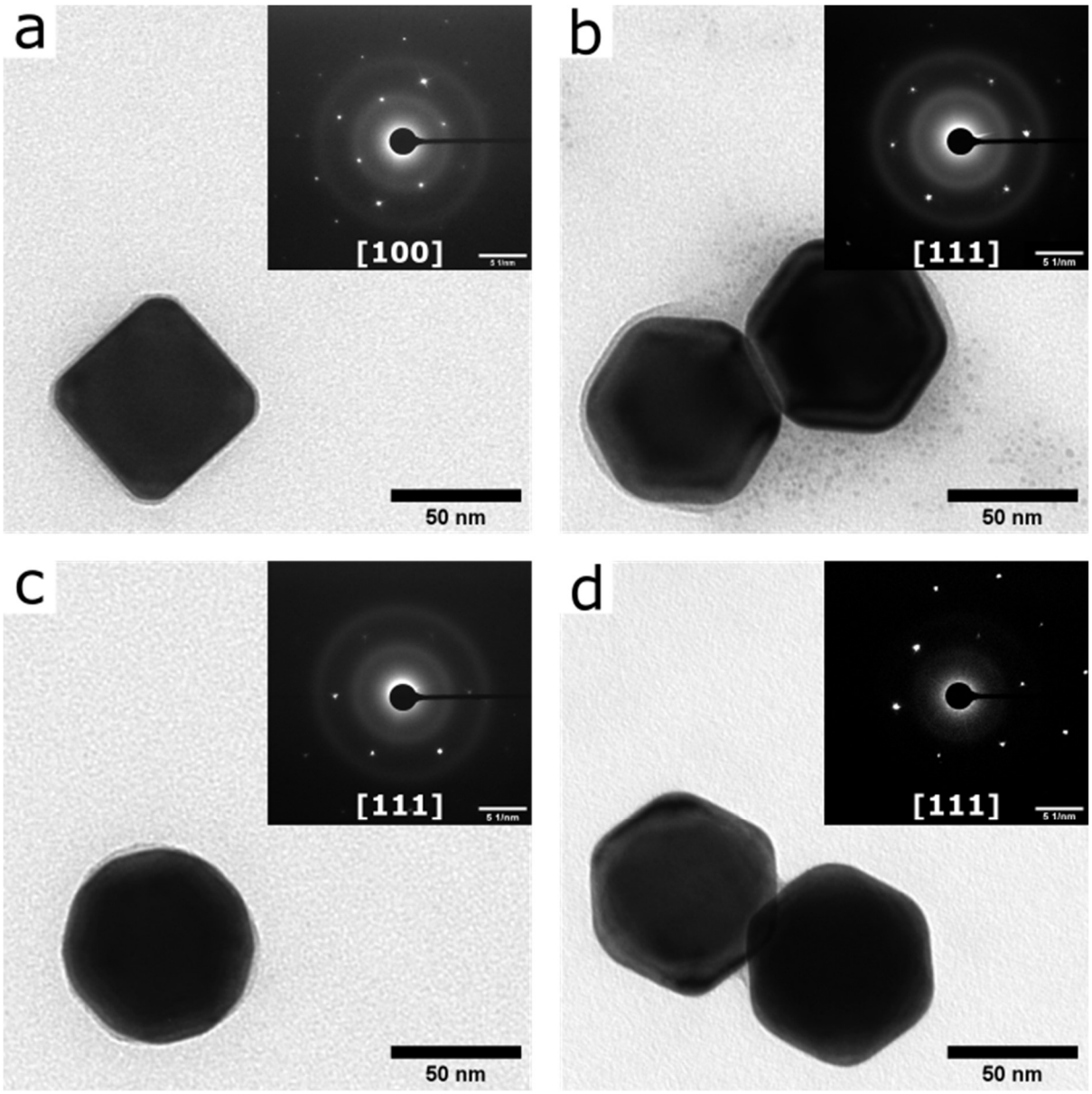

Figure S10. The single crystalline nature of the grown particles is proven by ED. Particles correspond to the ones depicted in Figure 3.

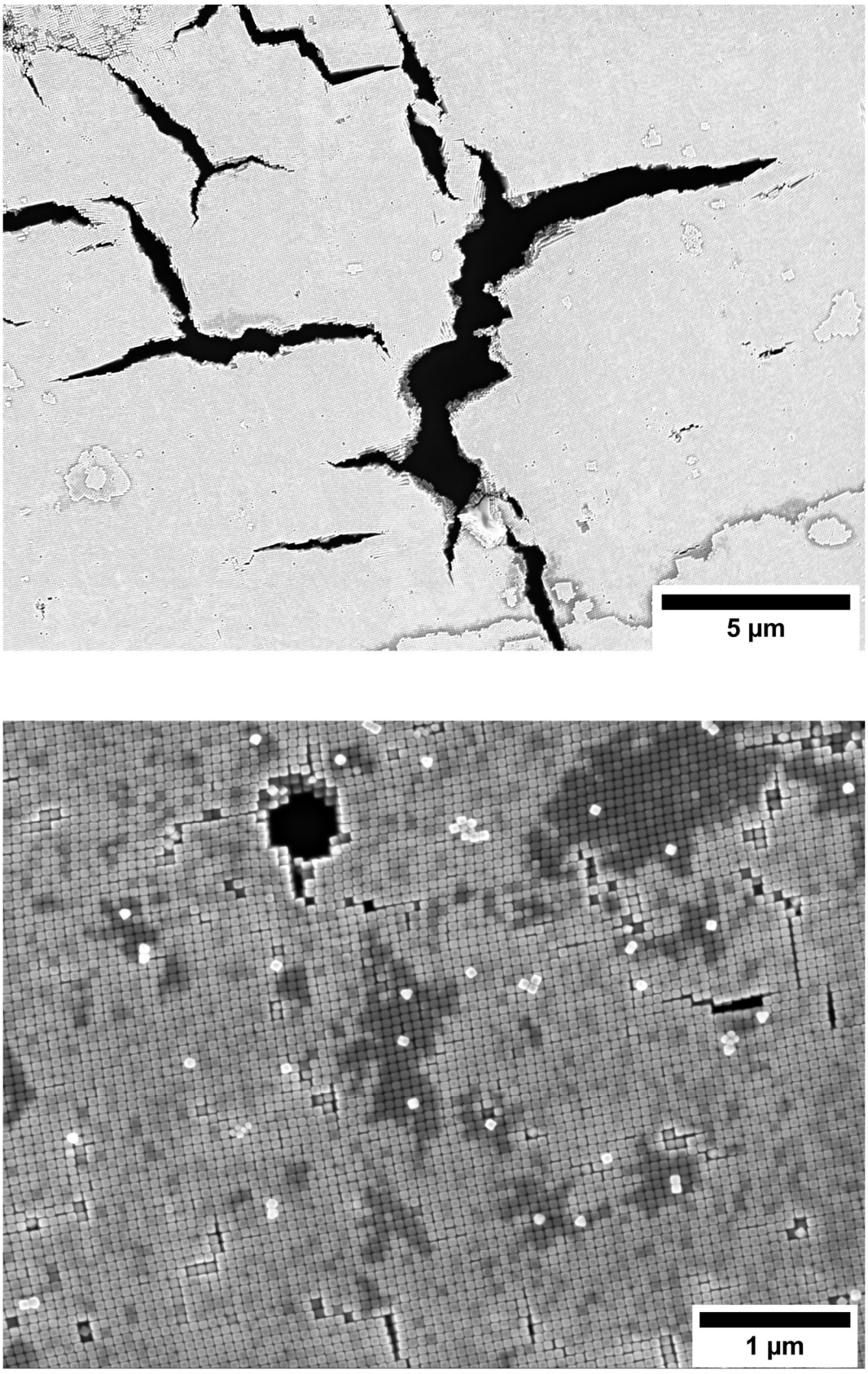

Figure S11. The quality of the particles can be shown using SEM. Assemblies are built from particles also shown in Figure 3a.

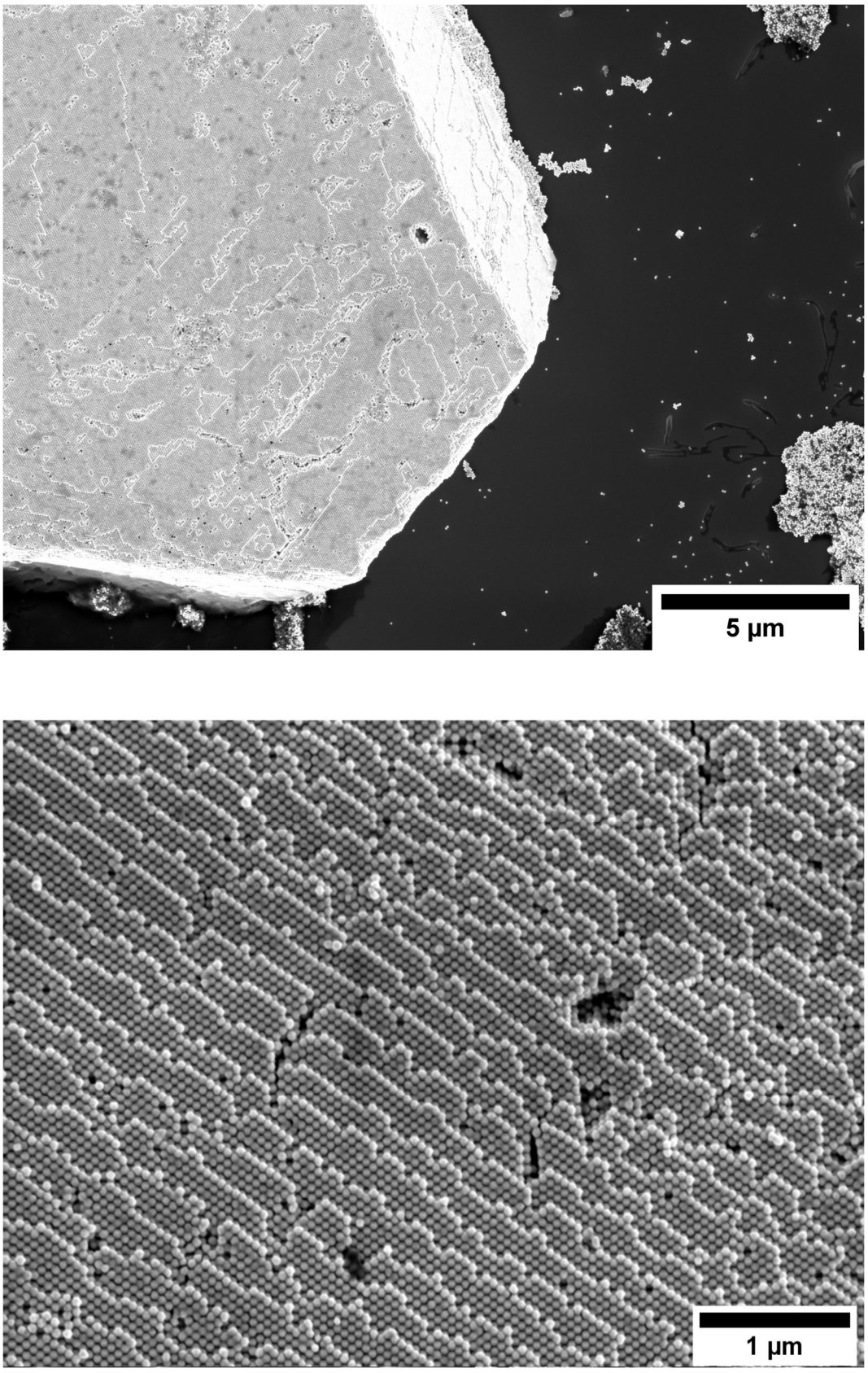

Figure S12. The quality of the particles can be shown using SEM. Assemblies are built from particles also shown in Figure 3b.

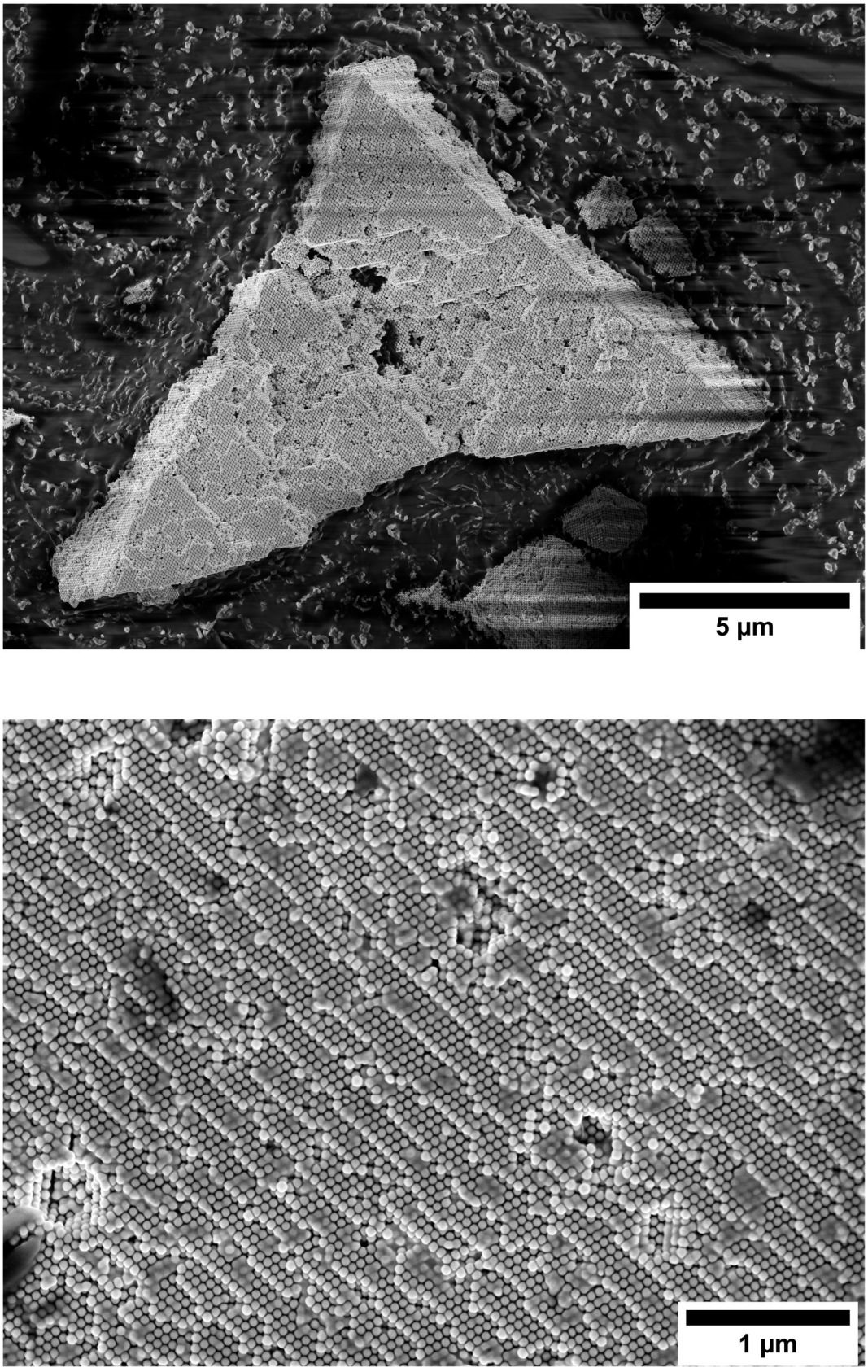

Figure S13. The quality of the particles can be shown using SEM. Assemblies are built from particles also shown in Figure 3c.

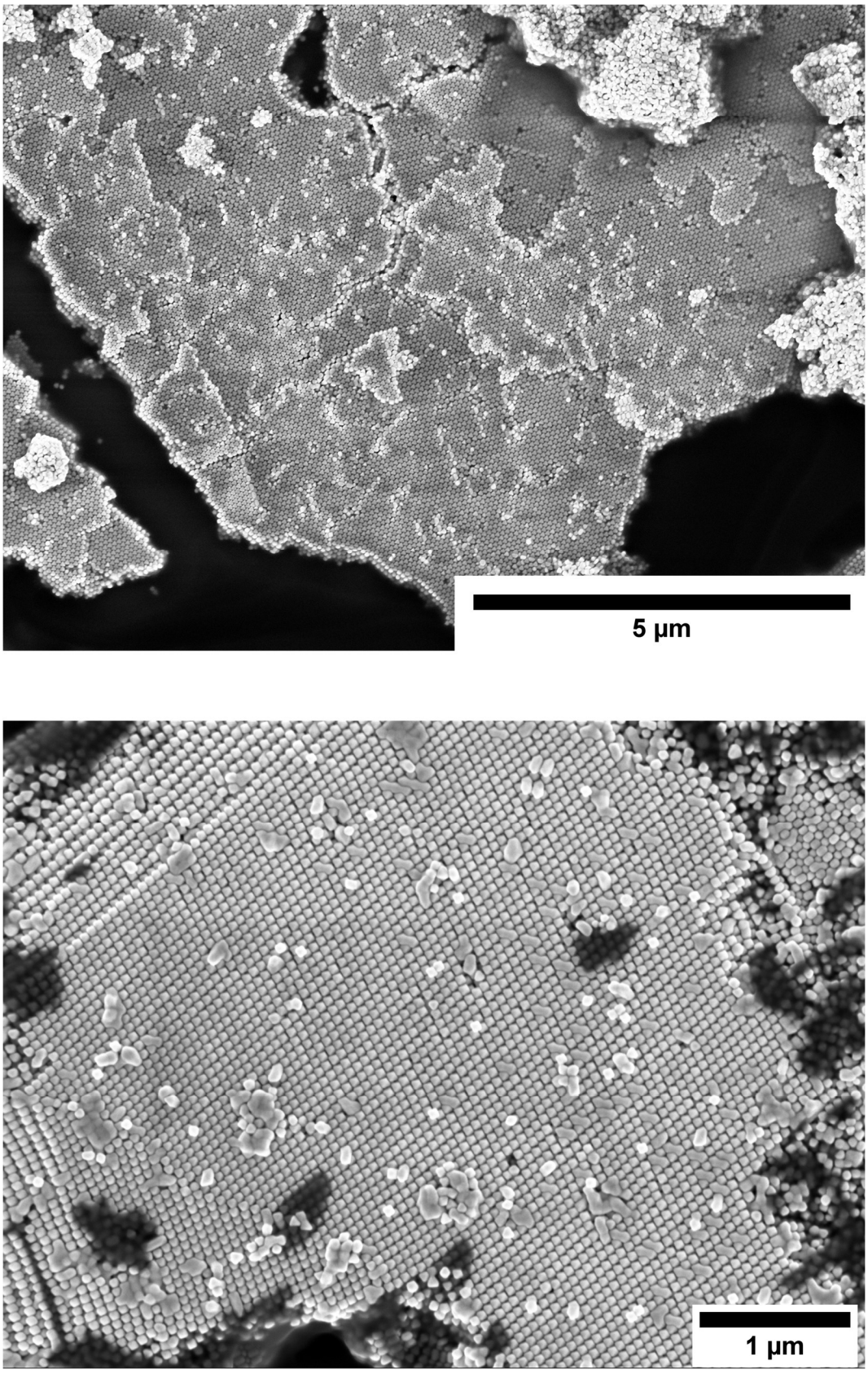

Figure S14. The quality of the particles can be shown using SEM. Assemblies are built from particles also shown in Figure 3d.

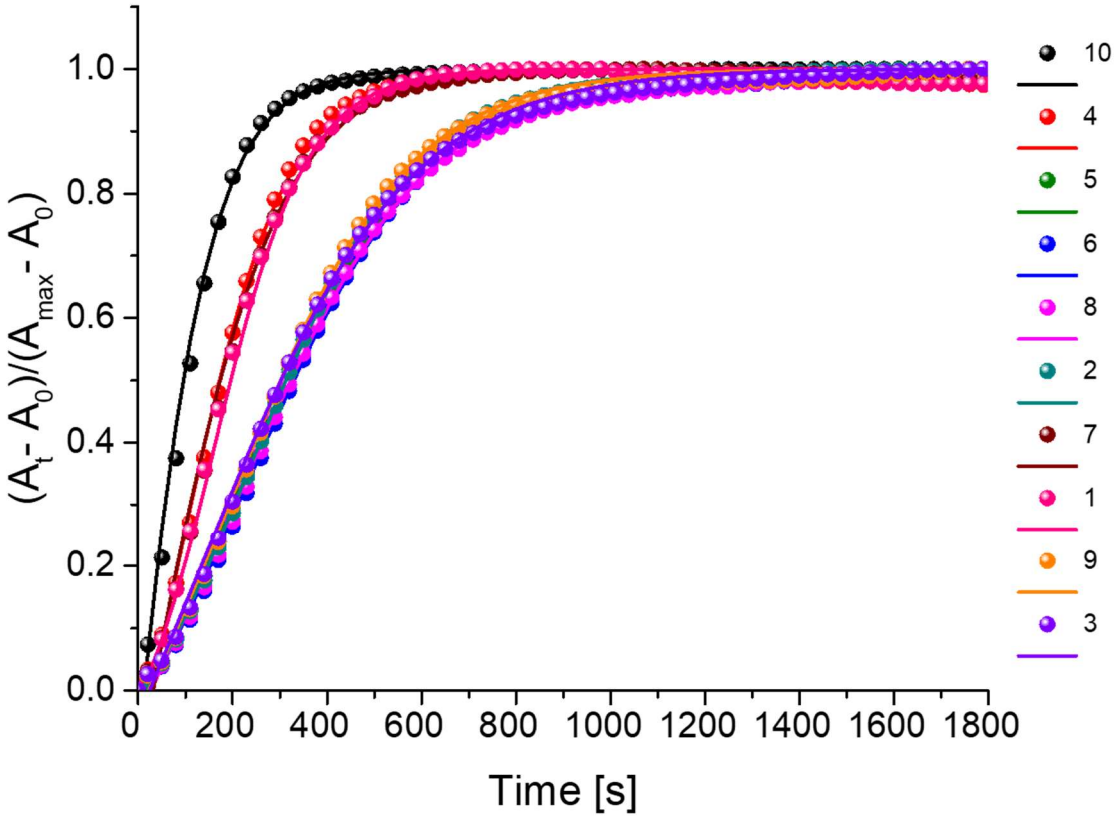

Sample No	a_0	a_1	a_2	$s(a_0)$	$s(a_0)$	$s(a_0)$	R^2	k_1	k_2
1	0.16489	-0.00986	0.00685	0.03000	0.00012	0.00034	0.99867	0.00178	30.21
2	0.13554	-0.00570	0.00391	0.00685	0.00004	0.00007	0.99976	0.00122	17.24
3	0.17389	-0.00476	0.00262	0.01390	0.00008	0.00015	0.99886	0.00164	11.55
4	0.28569	-0.00902	0.00452	0.02898	0.00009	0.00025	0.99921	0.00301	19.93
5	0.15977	-0.00500	0.00301	0.01070	0.00006	0.00012	0.99933	0.00147	13.27
6	0.25463	-0.00505	0.00292	0.01000	0.00007	0.00010	0.99928	0.00128	12.88
7	0.19232	-0.00759	0.00329	0.04000	0.00014	0.00044	0.99759	0.00360	14.51
8	0.27109	-0.00481	0.00258	0.01300	0.00008	0.00013	0.99884	0.00143	11.38
9	0.21449	-0.00544	0.00324	0.01200	0.00007	0.00012	0.99927	0.00142	14.29
10	0.17669	-0.01085	0.00298	0.06000	0.00037	0.00112	0.99609	0.00729	13.14

Figure S15. Normalized rate curves at λ_{max} obtained from UV-Vis spectra of samples in Figures 4. Points – experimental data; straight lines – fitted curves by Finke-Watzky autocatalytic two-step model based on procedure describes by Tatarchuk et al.[9-11] The calculated parameters of fitted curves (a_0, a_1, a_2, their standard deviations (s), and R^2) and k_1 and k_2 observed rate constants of the "pseudoelementary" reactions are listed in the table.

References

1. G. Gonzalez-Rubio, T. M. de Oliveira, T. Altantzis, A. La Porta, A. Guerrero-Martinez, S. Bals, L. Scarabelli and L. M. Liz-Marzan, *Chem Commun (Camb)*, 2017, **53**, 11360-11363.
2. G. Gonzalez-Rubio, V. Kumar, P. Llombart, P. Diaz-Nunez, E. Bladt, T. Altantzis, S. Bals, O. Pena-Rodriguez, E. G. Noya, L. G. MacDowell, A. Guerrero-Martinez and L. M. Liz-Marzan, *ACS Nano*, 2019, **13**, 4424-4435.
3. N. R. Jana, L. Gearheart and C. J. Murphy, *Adv. Mater.*, 2001, **13**, 1389-1393.
4. B. Nikoobakht and M. A. El-Sayed, *Chem. Mater.*, 2003, **15**, 1957-1962.
5. T. K. Sau and C. J. Murphy, *J. Am. Chem. Soc.*, 2004, **126**, 8648-8649.
6. X. Ye, L. Jin, H. Caglayan, J. Chen, G. Xing, C. Zheng, V. Doan-Nguyen, Y. Kang, N. Engheta, C. R. Kagan and C. B. Murray, *ACS Nano*, 2012, **6**, 2804-2817.
7. J. Schindelin, I. Arganda-Carreras, E. Frise, V. Kaynig, M. Longair, T. Pietzsch, S. Preibisch, C. Rueden, S. Saalfeld and B. Schmid, *Journal*, 2012, **9**, 676-682.
8. S. Gómez-Graña, B. Goris, T. Altantzis, C. Fernández-López, E. Carbó-Argibay, A. Guerrero-Martínez, N. Almora-Barrios, N. López, I. Pastoriza-Santos, J. Pérez-Juste, S. Bals, G. Van Tendeloo and L. M. Liz-Marzán, *The Journal of Physical Chemistry Letters*, 2013, **4**, 2209-2216.
9. V. V. Tatarchuk, Y. O. Dobrolyubova, I. A. Druzhinina, V. I. Zaikovskii, P. N. Gevko, E. A. Maksimovskii and S. A. Gromilov, *Russian Journal of Inorganic Chemistry*, 2016, **61**, 535-543.
10. V. V. Tatarchuk, A. P. Sergievskaya, I. A. Druzhinina and V. I. Zaikovsky, *Journal of Nanoparticle Research*, 2011, **13**, 4997.
11. V. V. Tatarchuk, A. P. Sergievskaya, T. M. Korda, I. A. Druzhinina and V. I. Zaikovsky, *Chem Mater*, 2013, **25**, 3570-3579.